UCRL-18759
cy. 2

EFFECT OF RADIOFREQUENCY FIELDS ON MÖSSBAUER SPECTRA

Helmut Gabriel

February 1969

LAWRENCE RADIATION LABORATORY
UNIVERSITY of CALIFORNIA BERKELEY

UCRL-18759
cy. 2

DISCLAIMER

To be submitted to Physical Review

UCRL-18759
Preprint

UNIVERSITY OF CALIFORNIA

Lawrence Radiation Laboratory
Berkeley, California 94720

AEC Contract No. W-7405-eng-48

EFFECT OF RADIOFREQUENCY FIELDS ON MÖSSBAUER SPECTRA

Helmut Gabriel

February 1969

EFFECT OF RADIOFREQUENCY FIELDS ON MÖSSBAUER SPECTRA*

Helmut Gabriel†

Lawrence Radiation Laboratory
University of California
Berkeley, California 94720

February 1969

ABSTRACT

The effect of a radiofrequency field on Mössbauer spectra is reconsidered. Both the ground and excited states of the source nuclei are simultaneously exposed to the rf magnetic field. As an example, the effect of the rf field on ^{57}Fe nuclei in a source with magnetic splitting (detected by a single-line absorber) is discussed in detail for two experimental geometries. Mössbauer spectra taken at a constant velocity, but with varying radiofrequency, show that the main features can be understood in terms of two-quantum processes (rf-induced transitions between the magnetic sublevels preceding or subsequent to the emission of a γ quantum), as long as the rf amplitude is small compared to the static magnetic field at the nucleus.

I. INTRODUCTION

The first theory of the influence of a radiofrequency (rf) field on the nuclear Zeeman lines has been given by Hack and Hammermesh,[1] whose treatment is an extension of the Weisskopf-Wigner theory of spontaneous emission. They give an expression for the emission-line shape for the case that the rf field acts only on the excited state of the nuclei. Recently, Mitin[2] investigated the problem of "gamma magnetic resonance" in a ferromagnet and calculated, using second-order perturbation theory, the effective absorption-cross section for two-quantum transitions (simultaneous absorption of a Mössbauer quantum and a quantum of the external rf field). No external constant magnetic field was assumed, and his final expression is for the Bloch wall activity in a fine powder of particles with several domains.

At the present time, it is by no means clear whether the pure rf resonance effect on the Mössbauer line shape has been observed at all. Heiman et al.[3] showed experimentally that in thin iron foils rf fields generate acoustical sidebands in the Mössbauer spectra and suggested that the resonance effect reported by Matthias[4] is due to sideband overlap with the normal Mössbauer lines. Perlow,[5] on the other hand, demonstrates the destruction of the Mössbauer hyperfine pattern by a non-resonant rf field and attributes the effect to rf-induced domain-wall motion causing alterations in the directions of hf fields. Both phenomena make it difficult to observe the rf resonance effect on the Mössbauer line shape in ferromagnetics. Working with single-domain samples still requires suppression of the disturbing influence of

magnetostriction. Besides solving the problem for Mössbauer isotopes in ferromagnets by appropriate experimental means it is worthwhile to investigate the possibilities of the rf method for isotopes with long-lived excited states in samples without magnetostriction. Matthias[4] has already mentioned that Mössbauer-NMR might become an experimental technique of high sensitivity. Particularly, a small line-width makes magnetic hf splitting observable in relatively small fields; therefore, a large ratio of the rf field amplitude to the dc magnetic field can be obtained without relying on the hyperfine enhancement which gives ferromagnets their favored position among host materials.

In the present paper the effects of the rf field on both the ground and excited states are treated on an equal footing. Since the total state of the decaying system is a coherent linear combination of the ground and the excited state, this is a natural procedure which leads to a very symmetric form of the emission spectrum. In Section II we sketch the theoretical approach used in this paper. Section III presents, for several experimental geometries and conditions, Mössbauer spectra (as a function of the velocity and, especially, as a function of the applied radiofrequency) which could be of help in designing conclusive Mössbauer-NMR experiments.

II. THE EMISSION SPECTRUM

The general expression for the Mössbauer emission spectrum

$$E(\omega_\lambda\ \underline{k}\ \underline{\varepsilon}) = \int_{-\infty}^{+\infty} e^{i(\omega_n - \omega_\lambda)t - \Gamma_s|t|/2}\ \mathrm{Tr}\left\{H_e^+(\underline{k},\ \underline{\varepsilon})\ \rho\ H_e(\underline{k},\ \underline{\varepsilon};\ t)\right\}dt \tag{1}$$

can also be used in the presence of the time-dependent rf field, if the Heisenberg operator $H_e(\underline{k},\ \underline{\varepsilon};\ t)$ describing the emission of a γ-quantum with wave vector $\underline{k}$ and polarization $\underline{\varepsilon}$ is defined by

$$H_e(t) = T\ \exp\left\{i\int_0^t L(\tau)\ d\tau\right\} H_e \qquad (\hbar = 1)\ . \tag{2}$$

The Liouville operator entering the time-ordered exponential is given by

$$L(t) = L_0 + L_1(t) \tag{3a}$$

$$L_0 = \sum_{\kappa=e,g} \omega_\kappa\ \hat{I}_{\kappa z}\ ,\quad \omega_\kappa = -\gamma_\kappa\ H_0\ , \tag{3b}$$

$$L_1(t) = (1/2)\sum_{\kappa=e,g} \omega_{1\kappa}\ [\hat{I}_{\kappa+}\ e^{-i\omega t} + \hat{I}_{\kappa-}\ e^{i\omega t}]\ ,\quad \omega_{1\kappa} = -\gamma_\kappa\ H_1\ . \tag{3c}$$

The unperturbed part (3b) describes the Zeeman splitting in a constant effective field H_0 (taken as quantization axis), whereas (3c) is due to the presence of a circularly polarized rf field with amplitude $H_1 \perp H_0$ and frequency ω. The Liouville operators L, $\hat{I}_z$ and $\hat{I}_\pm$ are defined

by the commutator equations $LX = [\mathcal{H}, X]$, $\hat{I}_z X = [I_z, X]$, etc., where $\mathcal{H}$ is the associated Hamiltonian and I_z, $I_\pm$ are the spherical components of the nuclear spin operator. (The Liouville operator algebra is reviewed in more detail in Refs. 6-8.) The labels e,g refer to excited and ground states, respectively.

Following the standard procedure a final expression for the emission spectra emerges from two subsequent steps: (1) Transformation to the rotating frame by the unitary operator

$$\hat{\Theta} = \exp\{i\omega t\,(\hat{I}_{ez} + \hat{I}_{gz})\} \tag{4}$$

and (2) rotation of the old z-axis $\parallel H_0$ to a new z"-axis coinciding with the resulting time-independent magnetic field in the Larmor frame. The appropriate rotation operator is denoted by $\hat{D}$. As a result we get the time-independent Liouville operator

$$L'' \equiv \hat{D}\,L'\,\hat{D}^+ \equiv \hat{D}\,\hat{\Theta}\,L\,\hat{\Theta}^+\,\hat{D}^+ = \sum_{\kappa=e,g} a_\kappa\,\hat{I}_{\kappa z''} \quad , \tag{5}$$

where

$$a_\kappa = \omega_\kappa\,[(1 + \omega/\omega_\kappa)^2 + (\omega_{1\kappa}/\omega_\kappa)^2]^{1/2} \tag{6}$$

is the precession frequency in the rotating frame. The transformed transition operator

$$H_e(t)' = \hat{\Theta}\,H_e(t) \tag{7}$$

obeys the equation of motion

$$\partial H_e(t)'/\partial t = i\, L'\, H_e(t)' \tag{8a}$$

which has the formal solution

$$H_e(t)' = \exp\{iL't\}\, H_e(0)' = \exp\{iL't\}\, H_e \ ,$$

$$L' = \hat{\Theta}\, L\, \hat{\Theta}^{+} = \sum_{\kappa=e,g} (\omega + \omega_\kappa)\, \hat{I}_{\kappa z} \ . \tag{8c}$$

The final form of the trace expression in (1) results immediately from the two transformation steps:

$$\mathrm{Tr}\{H_e^{+}\rho H_e(t)\} = \mathrm{Tr}\{H_e^{+}\rho\hat{\Theta}^{+} \exp(iL't) H_e\} = \mathrm{Tr}\{H_e^{+}\rho\hat{\Theta}^{+}\hat{D}^{+} \exp(iL''t)\, \hat{D} H_e\}$$

$$= \sum_{\text{all } m\text{'s}} (\rho H_e|m_e m_g)(m_e m_g|\hat{\Theta}^{+}|m_e m_g)(m_e m_g|\hat{D}^{+}|M_e M_g) \tag{9}$$

$$\times\, (M_e M_g|\exp(iL''t)|M_e M_g)(M_e M_g|\hat{D}|m_e' m_g')(m_e' m_g'|H_e) \ .$$

The magnetic quantum numbers m_κ, m_κ' (M_κ) refer to the z-(z"-) axis as quantization direction. The basis vectors $|m_e m_g)$ in Liouville space have been used to break up the product of operators in (9). The operators $\hat{\Theta}$ and L'' are diagonal in the laboratory and rotating frame, respectively. The corresponding matrix elements follow immediately from the fact that the eigenvalues of a Liouville operator are just the differences of all eigenvalues of the ordinary operator with which it is associated

(see Refs. 6-8 for details). The matrix elements of the rotation operator $\hat{D}$ are products of the usual rotation matrices $\mathcal{D}^{(I)}_{mm'}(\alpha, \beta, \gamma)$. In our representation we get

$$(m_e m_g |\hat{D}^{+}| M_e M_g) = (\mathcal{D}^{-1})^{(I_e)}_{m_e M_e} \mathcal{D}^{(I_g)}_{M_g m_g} \tag{10a}$$

$$(M_e M_g |\hat{D}| m'_e m'_g) = \mathcal{D}^{(I_e)}_{M_e m'_e} (\mathcal{D}^{-1})^{(I_g)}_{m'_g M_g} \quad . \tag{10b}$$

In our special case we are left with only one rotation angle β_K ($\alpha_K = \gamma_K = 0$), for each of the two states, given by

$$a_K \sin \beta_K = \omega_{1K} \quad ; \quad a_K \cos \beta_K = \omega_K + \omega \quad . \tag{11}$$

Therefore, only the $d^{(I)}_{mm'}(\beta)$ matrices enter the final expression

$$\Phi_s(t) \equiv \mathrm{Tr}\{H_e \rho H_e(t)\} = \sum_{\substack{m_e m'_e \\ m_g m'_g}} \langle m'_e|H_e|m'_g\rangle \langle m_e|\rho H_e|m_g\rangle^{*}$$

$$\times \sum_{M_e M_g} \exp\left[it\{a_e M_e - a_g M_g - \omega(m_e - m_g)\}\right] \tag{12}$$

$$\times \left[d^{(I_e)}_{M_e m'_e}(\beta_e)\, d^{(I_e)}_{M_e m_e}(\beta_e)\right]\left[d^{(I_g)}_{M_g m_g}(\beta_g)\, d^{(I_e)}_{M_g m'_g}(\beta_g)\right] \quad ,$$

which inserted in (1), determines the intensity distribution of the emitted radiation under the influence of the rf field.

In the case of equal populations ($\rho = (2I_e+1)^{-1} \cdot 1$) and polycrystalline sources (only terms with $m_e' = m_e$ are non-zero) each component in (12) reduces to Hack and Hammermesh's result,[9] if we neglect the influence of the rf on the ground state ($\omega_{1g} = 0$; $d^{(I_g)}_{M_g m_g}(\beta_g = 0) = \delta_{M_g m_g}$). Equation (12) could be given another form by expressing the action of the rf field in terms of resultant time-dependent rotation matrices and introducing the Majorana factors well known from NMR theory.[10] However, since the Mössbauer emission spectrum is the Fourier transform of $\Phi_s(t)$, the form (12) is most convenient. The spectrum is simply given as a superposition of Lorentzians with modified resonance frequencies and rf-dependent intensities (see also Section III).

III. TYPICAL EXAMPLES OF MÖSSBAUER SPECTRA

The experimentally observed ω-dependent Mössbauer spectrum is given by

$$M(v;\omega) \propto \sum_{\underline{\varepsilon}} \int_{-\infty}^{+\infty} d\omega_\lambda \; E(\omega_\lambda, \underline{k}, \underline{\varepsilon}) \; A(\omega_\lambda - v\omega_n', \underline{k}, \underline{\varepsilon}) \quad (c=1) \; . \tag{13}$$

The summation over $\underline{\varepsilon}$ indicates that polarization is not observed and $A(\omega_\lambda)$ is the properly chosen absorption cross section. (ω_n' is the unsplit transition frequency in the absorber. The integral (13) is simply evaluated for Lorentzian line shapes.

The following cases have been chosen to illustrate the modification of the line pattern:

(1) A single-line absorber and a source with magnetic hf splitting and in the presence of an rf field;

(2) split abosrber and split source, the latter exposed to the rf field.

Allowing for an isomer shift $\Delta = \omega_n - \omega_n'$ between source and absorber, the Mössbauer spectrum for Example (1) reads

$$M(v;\omega) \propto \sum_{m_e m_g} \begin{pmatrix} I_e & L & I_g \\ -m_e & m_e - m_g & m_g \end{pmatrix}^2 F^{LL}_{m_e - m_g}(\theta) L(m_e m_g;\omega) \; ,$$

$$L(m_e m_g;\omega) = \sum_{M_e M_g} [d^{(I_e)}_{M_e m_e}(\beta_e)]^2 \; [d^{(I_g)}_{M_g m_g}(\beta_g)]^2 \; \times$$

$$\times \frac{1}{\pi} \cdot \frac{\Gamma}{[v- \{\Delta-\omega(m_e-m_g) + a_e M_e - a_g M_g\}]^2 + \Gamma^2} \quad , \tag{14}$$

$$\Gamma = (1/2)(\Gamma_s + \Gamma_a) \quad .$$

The coefficients $F^{LL}_{m_e-m_g}(\theta)$ are tabulated.[11] They determine the angular distribution of the radiation as a function of the angle $\theta = \sphericalangle(\underline{k}, \underline{H}_0)$. Figure 1 shows ^{57}Fe velocity spectra for $\theta = 90°$ and several frequencies. The changes in the line shape due to the radiofrequency are shown in more detail for the inner pair of lines and $\theta = 0°$ in Fig. 2. These curves display the splitting of each line into maximally $(2I_K + 1)$ components.[1] Hack and Hammermesh give plots for individual split lines, whereas Figs. 1-2 show the superposition of all of them. According to the transformation operator (4), the radiofrequency is formally allowed to assume positive and negative values. The resonance frequencies for ^{57}Fe in ferromagnetic iron are, therefore, at $\nu_{res}(e) = -26$ MHz and $\nu_{res}(g) = 45.4$ MHz. In cases like ^{57}Fe, where the gyromagnetic ratios differ not only in magnitude but even in sign, a circularly polarized rf field acting on the emitter nuclei affects either the excited or the ground state (depending on the sense of rotation). For linearly polarized rf fields a superposition of both effects is expected. However, since the intensity of the off-resonance terms drops to zero with increasing deviation from resonance, a velocity spectrum at fixed radiofrequency will show significant overlap of ground and excited state effects only if the rf is near resonance for both levels, i.e. only if the gyromagnetic ratios are of comparable magnitude. The preceding

remarks also explain why the maximum multiplicity of the single lines is practically always given by $(2I_e + 1)$ or $(2I_g + 1)$ and not by $(2I_e + 1) \times (2I_g + 1)$ as it should be according to (15).

Figures 3 and 4 show, still for case (1) and for zero velocity, the frequency dependence of the Mössbauer spectra. If there is no shift of the absorber line relative to the pattern of the split emitter, the experimental setup of case (1) is, of course, most unfavorable because of the low intensity of the absorption spectrum at $v = 0$. However, the physical processes are easily understood for this case and the following remarks apply, slightly modified, also to other experimental geometries.

The rf field enhances the absorption at $v = 0$ if no sufficiently large isomer shift Δ is present (see Fig. 3 ($\Delta = 0$)). This is obvious from the line shape changes shown in Fig. 2. The main contributions to the intensity increase at $v = 0$ stem from the inner rf-split lines, the satellites of which are swept over the absorption line in a certain frequency range. Most of the peaks in the resulting pattern can be interpreted as two-quantum transition, i.e. in terms of second-order perturbation theory. For small values of β the rotation matrices can be approximated by

$$d^{(I)}_{Mm}(\beta) \equiv \langle M|\exp(i\beta I_y)|m\rangle \approx \delta_{M,m} + (\beta/2)\langle M|I_+ - I_-|m\rangle \qquad (15)$$

which tells us that, due to the last term in (15) (proportional to $\delta_{M,m\pm1}$), forbidden transitions contribute to the spectrum. For magnetic dipole transitions with $|\Delta m| = |m_e - m_g| = 0,1$ we have, under the influence of the rf field, additional transitions with $|\Delta m| = 2$. Using (15), the

line shape function $L(m_e m_g;\omega)$ of Eq. (14) may be written as

$$L(m_e m_g;\omega) \approx L(m_e m_g;0)+(\Gamma/4\pi) \sum_{\varepsilon=\pm 1} \Big[\beta_e^2 \, r_\varepsilon(e)^2 \times \{[\nu - \Delta - \varepsilon\omega - (m_e+\varepsilon)\omega_e + m_g\omega_g]^2 + \Gamma^2\}^{-1} + \beta_g^2 \, r_\varepsilon(g)^2 \{[\nu - \Delta + \varepsilon\omega - m_e\omega_e + (m_g+\varepsilon)\omega_g]^2 + \Gamma^2\}^{-1} \Big] \quad (16)$$

with

$$r_e(\kappa)^2 = I(I+1) - m_\kappa(m_\kappa+\varepsilon) \quad ; \quad \beta_\kappa \approx \omega_{1\kappa}[(\omega+\omega_\kappa)^2 + \omega_{1\kappa}^2]^{-1/2} \, . \quad (17)$$

The frequency dependent part of (16) has maxima at $\nu_{max} = -16.3$ and -35.7 MHz due to induced emission and absorption of a rf quantum in the excited state and subsequent γ emission. The peak at $\nu_{max} = 35.7$ MHz (Fig. 3) is caused by rf induced transitions in the ground state. According to the experimental geometry ($\nu = 0$, $\Delta = 0$), the main contributions are due to the $(\pm \frac{1}{2} \rightarrow \mp \frac{1}{2})$ γ transitions, both for $\theta = 0°$ and $\theta = 90°$. For the latter angle two further lines originate from the $(\pm \frac{1}{2}, \mp \frac{1}{2})$ γ - transitions. They are centered at $\nu_{max} = 9.7$ MHz (rf transitions in both ground and excited state contribute to this line causing a relative intensity comparable to the inner pairs contribution) and at $\nu_{max} = -61.7$ MHz (a pure excited state rf effect). The relative intensities can be estimated from the associated values of β_κ^2 using (17). (In the approximate expression for β_κ, the frequencies $\omega_{1\kappa}$ have been retained in the

denominator in order to avoid singularities at $\omega = -\omega_K$; see, as an example, Mitin's final result.)

For the selected values of $H_1/H_0 \leq 10^{-1}$, the frequency curves (Figs. 3-4) calculated from the exact formula (14) are remarkably well described by a perturbation approach. In our example, only the small peaks (marked by arrows in Fig. 3) at frequencies $\nu_{max} = -8.1$ MHz and $+30.8$ MHz are typical higher than second-order contributions ($|\Delta m| = 3$). All frequencies ν_{max} mentioned above can be calculated from the formula

$$\omega = \frac{\omega_g M_g - \omega_e M_e}{(m_e - m_g + M_e - M_g)}$$

which follows directly from Eq. (14) if we neglect $(H_1/H_0)^2$ in the denominator. The quoted second-order perturbation results were found for $(M_g = m_g,\ M_e = m_e \pm 1)$ and $(M_g = m_g \pm 1,\ M_e = m_e)$.

We now turn to the discussion of Fig. 4 calculated for zero velocity, but with a hypothetical isomer shift of $\Delta = 35.7$ MHz. The absorber line has been shifted to the position of the strongest emitter line ($\theta = 90°$), thus increasing the base line intensity with respect to the $v = \Delta = 0$ case by a factor of 200, and the relative rf effect by a factor of 2. Because of the symmetric situation, the frequency spectrum has only two lines at the ground and excited state resonance frequencies. The rf field leads to a decrease in the absorption, because, in a certain frequency interval, the emitter line is flowing out of the region where the absorber line is located. The case under

discussion can be considered a model for a realistic experimental situation. Since it is irrelevant for the study of the rf effect how overlap of two appropriate absorber and emitter lines is accomplished, we can look for cases where the hf pattern is shifted by a Zeeman drive. (For an example of the latter technique, see Sauer, Matthias, and Mössbauer.[12])

Figure 5 shows a Mössbauer frequency spectrum for case (2). It is unnecessary to discuss the details of the split source-split absorber case because nothing basically new can be learned as compared to example (1). For systems without any isomer shift, the rf effect is expected to be considerably larger for case (2).

ACKNOWLEDGMENTS

It is a pleasure to thank Professor D. A. Shirley for his hospitality during my stay at the Lawrence Radiation Laboratory. Numerous discussions with Drs. E. Matthias and D. Quitmann and Dr. M. Salomon are gratefully acknowledged. I also wish to express my gratitude to Mr. D. Salomon for writing the computer program. This work was carried out during the tenure of a Fellowship for which I am indebted to the Max Kade Foundation.

FOOTNOTES AND REFERENCES

*Work performed under the auspices of the U. S. Atomic Energy Commission.

†On leave from Institut für Theoretische Physik A, Technische Universität Braunschweig.

1. M. N. Hack and M. Hammermesh, Nuovo Cimento 19, 546 (1961).
2. A. V. Mitin, Zh. eksper. theor. Fiz. 52, 1596 (1967); [Translation: JETP 25, 1062 (1967)].
3. N. D. Heiman, L. Pfeiffer, and J. C. Walker, Phys. Rev. Letters 21, 93 (1968).
4. E. Matthias, Hyperfine Structure and Nuclear Radiations, edited by E. Matthias and D. A. Shirley (North-Holland Publishing Company, Amsterdam, 1968) p. 815.
5. G. J. Perlow, Phys. Rev. 172, 319 (1968).
6. R. Zwanzig, Physica 30, 1109 (1964).
7. H. Gabriel, J. Bosse, and K. Rander, Phys. Stat. Sol. 27, 301 (1968).
8. M. Blume, Phys. Rev. 174, 351 (1968).
9. The notation in Eq. (32), reference 1 is misleading. The frequency ω_0 actually refers to an individual transition between the hf split levels and should be labeled by the particular magnetic quantum of the excited state.
10. H. Salwen, Phys. Rev. 99, 1274 (1955).
11. L. W. Fagg and S. S. Hanna, Rev. Mod. Phys. 31, 711 (1959); see Table VI (b).
12. C. Sauer, E. Matthias, and R. L. Mössbauer, Phys. Rev. Letters 21, 961 (1968).

FIGURE CAPTIONS

Fig. 1. Velocity spectra of ^{57}Fe in a source with magnetic splitting (H_0 = 330 kOe) exposed to various radiofrequencies versus a single-line absorber. ($\underline{H}_0 \perp \underline{k}$, Γ = 1.1 MHz)

Fig. 2. Velocity spectra covering the inner pair of lines under the same conditions as in Fig. 1 except that ($\underline{H}_0 \parallel \underline{k}$).

Fig. 3. Frequency spectra at zero velocity for various ratios H_1/H_0 under the same conditions as in Fig. 1. Arrows indicate frequencies at which multiple transitions occur.

Fig. 4. Frequency spectra at zero velocity for various ratios H_1/H_0 under the conditions of Fig. 1 but with an "isomer shift" Δ = 35.7 MHz.

Fig. 5. Frequency spectra at zero velocity for various ratios H_1/H_0 with source conditions as in Fig. 1 but with a magnetically split absorber ($\underline{H}_0 \parallel \underline{k}$).

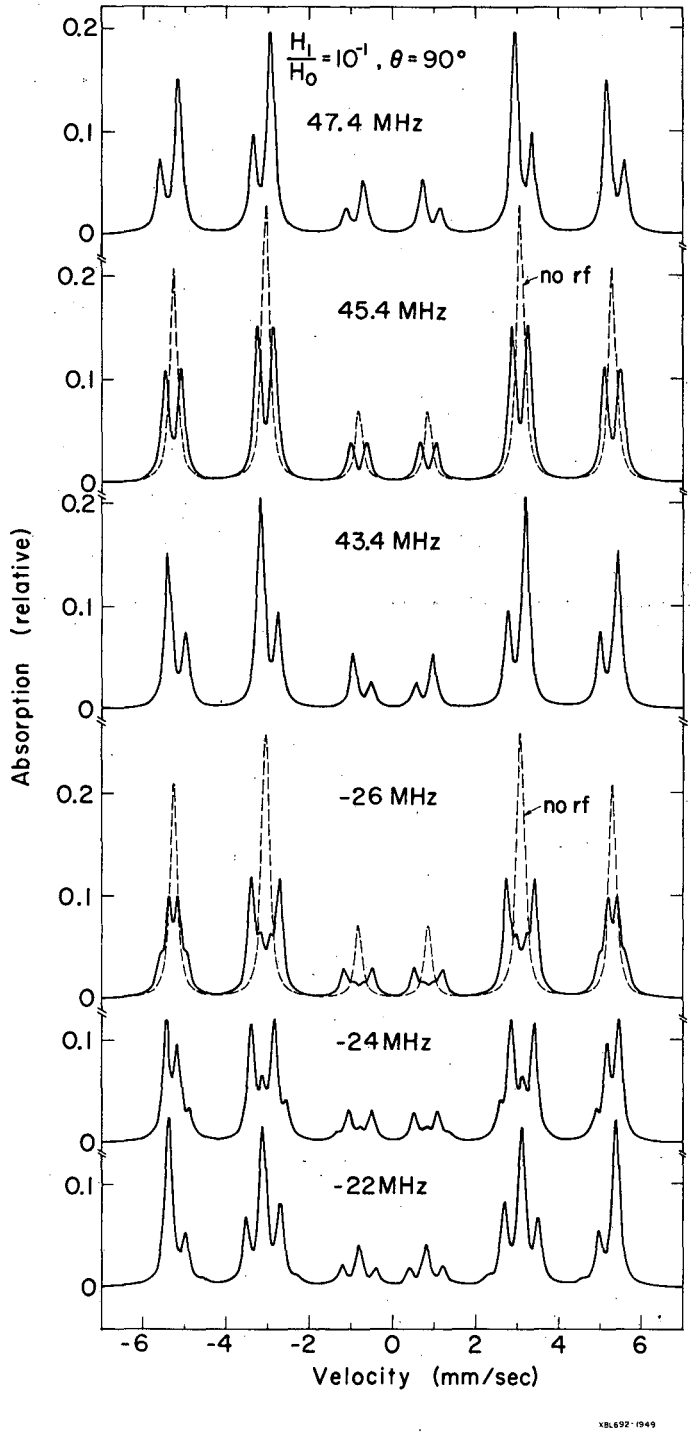
$\frac{H_1}{H_0} = 10^{-1}$, $\theta = 90°$
47.4 MHz
45.4 MHz
no rf
43.4 MHz
-26 MHz
no rf
-24 MHz
-22 MHz
0.2
0.1
0
-6
-4
-2
0
2
4
6
Absorption (relative)
Velocity (mm/sec)
XBL692-1949

Fig. 1.

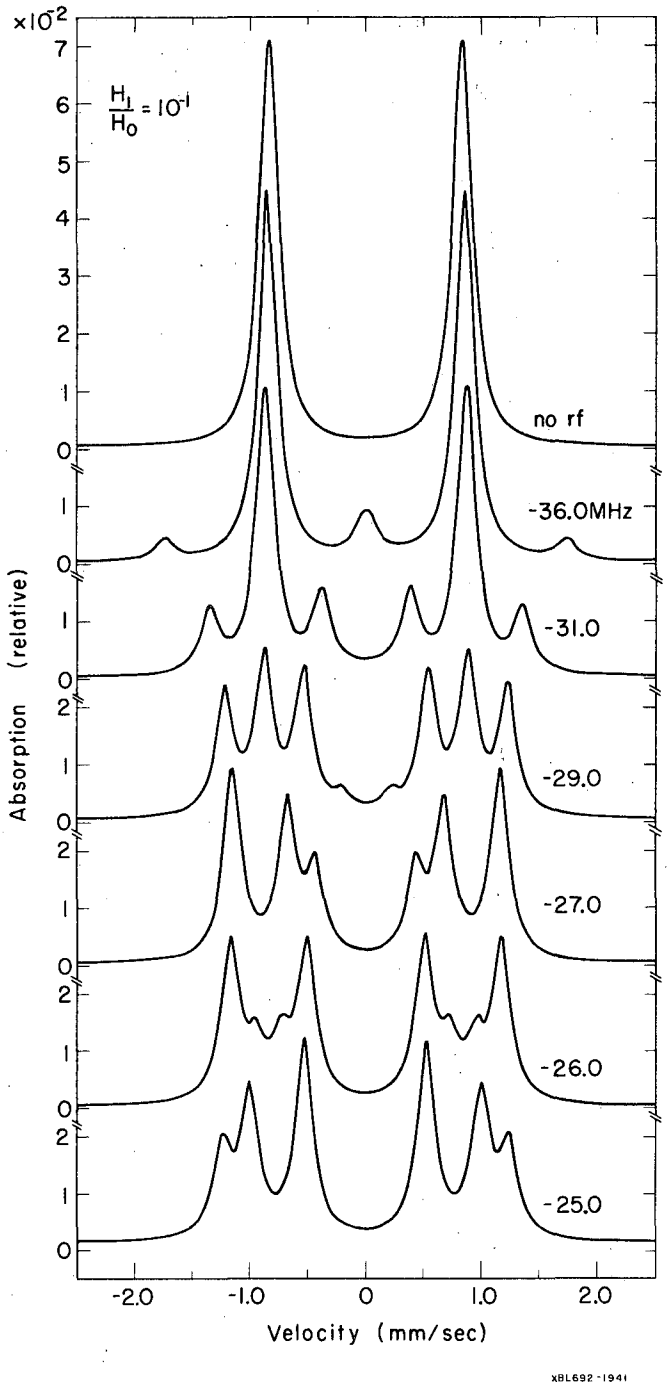
×10²
7
6
5
4
3
2
1
0
H1/H0 = 10⁻¹
no rf
-36.0MHz
-31.0
-29.0
-27.0
-26.0
-25.0
Absorption (relative)
-2.0
-1.0
0
1.0
2.0
Velocity (mm/sec)
XBL692-1941

Fig. 2.

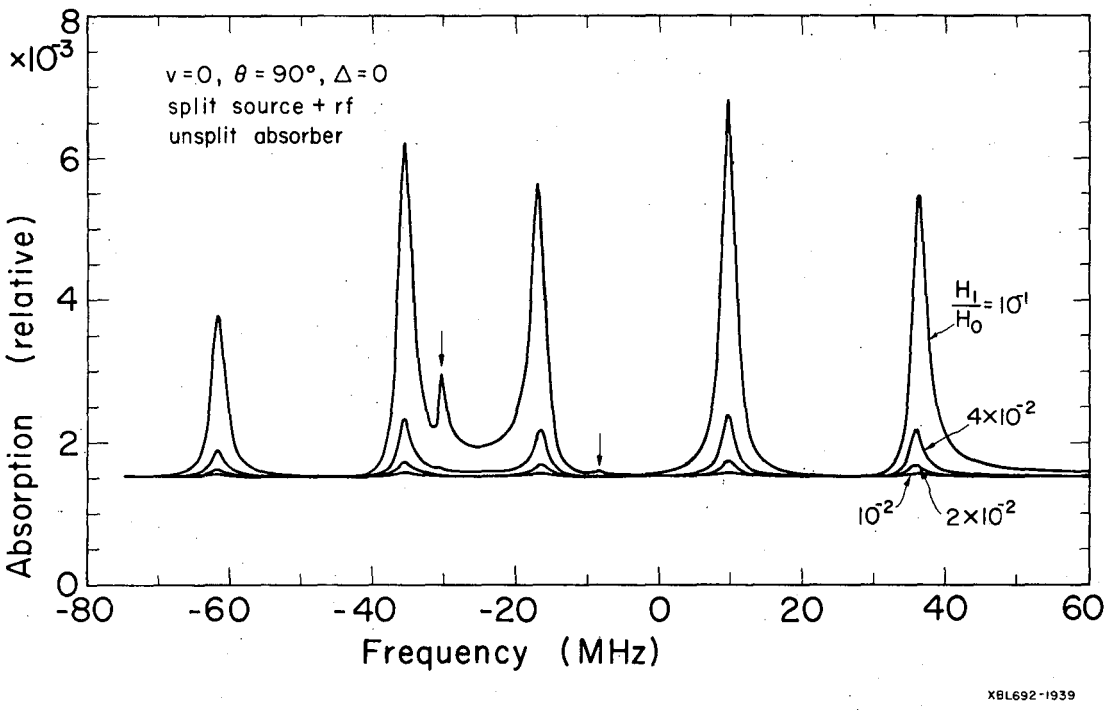
v = 0, θ = 90°, Δ = 0
split source + rf
unsplit absorber
×10⁻³
Absorption (relative)
Frequency (MHz)
H1/H0 = 10⁻¹
4×10⁻²
10⁻²
2×10⁻²
XBL692-1939

Fig. 3.

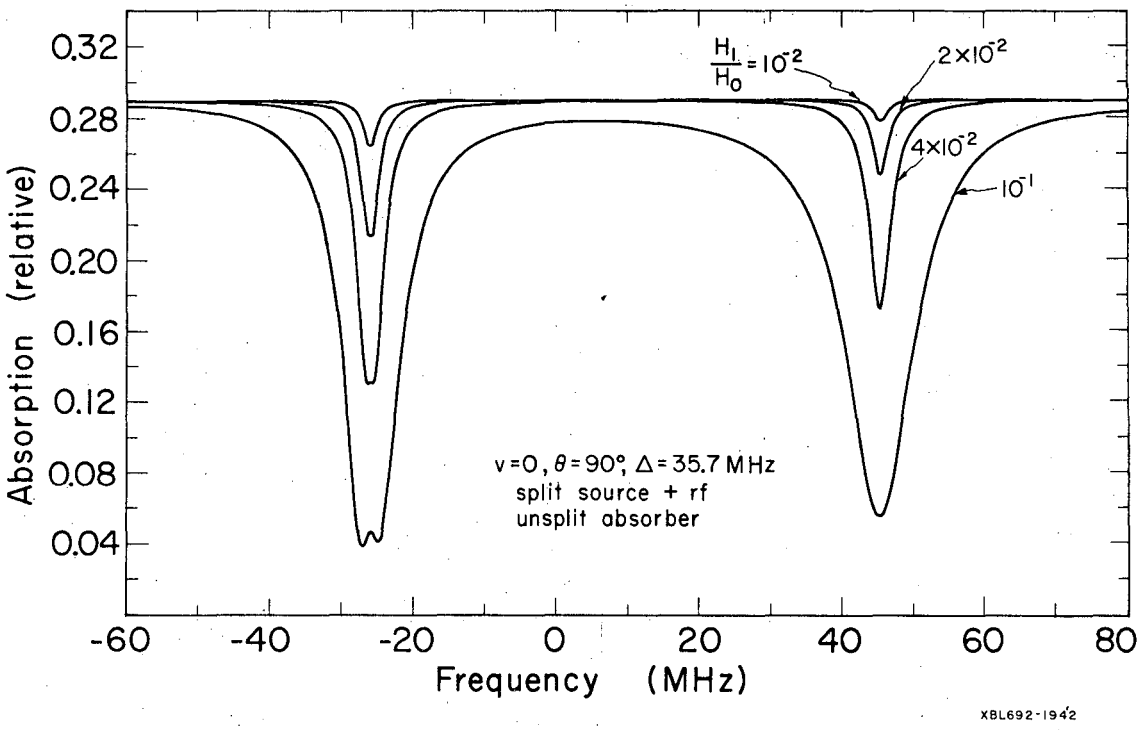
0.32
0.28
0.24
0.20
0.16
0.12
0.08
0.04
Absorption (relative)
$\frac{H_1}{H_0} = 10^{-2}$
2×10^{-2}
4×10^{-2}
10^{-1}
v=0, θ=90°, Δ=35.7 MHz
split source + rf
unsplit absorber
-60
-40
-20
0
20
40
60
80
Frequency (MHz)
XBL692-1942

Fig. 4.

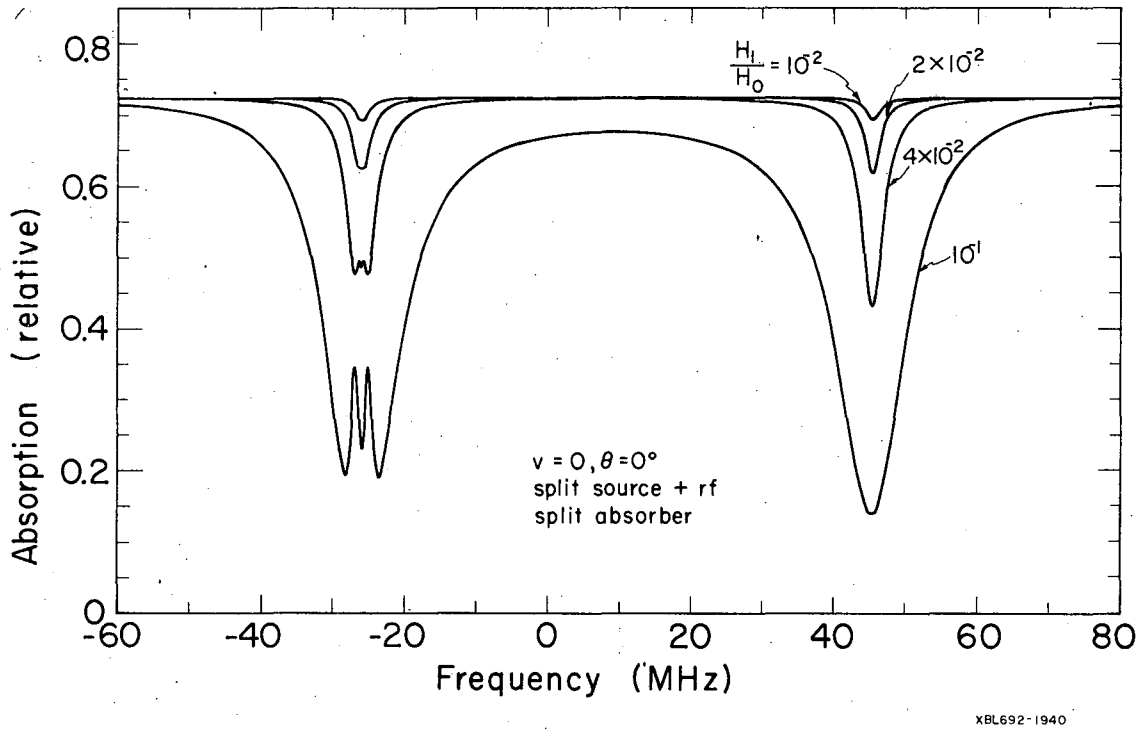
0.8
0.6
0.4
0.2
0
Absorption (relative)
$\frac{H_1}{H_0} = 10^{-2}$
2×10^{-2}
4×10^{-2}
10^{-1}
v = 0, θ = 0°
split source + rf
split absorber
-60
-40
-20
0
20
40
60
80
Frequency (MHz)
XBL692-1940

Fig. 5.

LEGAL NOTICE

TECHNICAL INFORMATION DIVISION
LAWRENCE RADIATION LABORATORY
UNIVERSITY OF CALIFORNIA
BERKELEY, CALIFORNIA 94720